J|A|C|S
ARTICLES

Published on Web 12/04/2008

Highly Regioselective Derivatization of Trimetallic Nitride Templated Endohedral Metallofullerenes via a Facile Photochemical Reaction

Chunying Shu, Carla Slebodnick, Liaosa Xu, Hunter Champion, Tim Fuhrer, Ting Cai, Jonathan E. Reid, Wujun Fu, Kim Harich, Harry C. Dorn,* and Harry W. Gibson*

Department of Chemistry, Virginia Polytechnic Institute and State University, Blacksburg, Virginia 24060-0212

Received June 26, 2008; E-mail: hwgibson@vt.edu; hdorn@vt.edu

Abstract: Photochemically generated benzyl radicals react with $Sc_3N@C_{80}$-I_h to produce a dibenzyl adduct [$Sc_3N@C_{80}(CH_2C_6H_5)_2$] in 82% yield and high regioselectivity. The adduct's ^1H spectrum revealed high symmetry: only one AB pattern was observed for the methylene protons. The ^{13}C NMR spectrum suggested a C_2-symmetrical structure. DFT calculations reveal that a 1,4-adduct is more favorable than a 1,2-adduct by >10 kcal/mol. The 1,4-structure on [566] ring junctions was unambiguously confirmed by X-ray crystallographic analysis. UV−vis spectra revealed that the removal of two p orbitals from the π system of the cage together with the benzylic substituents change the electronic properties of the metallofullerene in a manner similar to those reported for disilirane and trifluoromethyl moieties. Under the same conditions from $Lu_3N@C_{80}$-I_h we prepared (63% yield) $Lu_3N@C_{80}(CH_2C_6H_5)_2$, which demonstrated properties similar to the 1,4-dibenzyl adduct of $Sc_3N@C_{80}$-I_h.

Introduction

Endohedral metallofullerenes (EMFs) have attracted special interest due to their unique properties relative to empty fullerenes.[1−4] Exploring new ways to functionalize trimetallic nitride templated (TNT) endohedral metallofullerenes with good solubility and processability is crucial for expanding their potential applications in material science and medicine.[2,3,5,6] However, to date, only a limited number of reactions of EMFs have been investigated to alter their exohedral character and physical properties. Notably, the TNT metallofullerenes,[7,8] formed in relatively high yields, lower only than C_{60} and C_{70} in the Krätschmer−Huffman electric-arc generator, are less reactive than classical EMFs due to the formal transfer of six electrons from the metal atoms to the fullerene cage, which leads to a closed shell electronic structure and an increase of the HOMO−LUMO gap with corresponding reduction in reactivity.[9,10] Most of their reactions are still limited to cycloadditions, such as [4 + 2] Diels−Alder reactions,[11−13] 1,3-dipolar additions,[14−21] and Bingel reactions.[22−24] The first noncycloaddition reaction was reported by Iezzi et al.[25] Very recently, cycloaddition[26] and noncycloaddition reactions[27] of $Sc_3N@C_{80}$-I_h, the isomer with icosahedral symmetry, with radicals were reported.

(1) Heath, J. R.; O'Brien, S. C.; Zhang, Q.; Liu, Y.; Curl, R. F.; Tittel, F. K.; Smalley, R. E. *J. Am. Chem. Soc.* **1985**, *107*, 7779–7780.
(2) Shinohara, H. *Rep. Prog. Phys.* **2000**, *63*, 843–892.
(3) Akasaka, T.; Nagase, T., Eds. *Endofullerenes: A New Family of Carbon Clusters*; Kluwer Academic Publishers: Dordrecht, 2002.
(4) Dunsch, L.; Yang, S. *Small* **2007**, *3*, 1298–1320.
(5) Thilgen, C.; Diederich, F. *Chem. Rev.* **2006**, *106*, 5049–5135.
(6) Martin, N. *Chem. Commun.* **2006**, 2093–2104.
(7) Stevenson, S.; Rice, G.; Glass, T.; Harich, K.; Cromer, F.; Jordan, M. R.; Craft, J.; Hadju, E.; Bible, R.; Olmstead, M. M.; Maitra, K.; Fisher, A. J.; Balch, A. L.; Dorn, H. C. *Nature* **1999**, *401*, 55–57.
(8) Krause, M.; Kuzmany, H.; Georgi, P.; Dunsch, L.; Vietze, K.; Seifert, G. *J. Chem. Phys.* **2001**, *115*, 6596–6605.
(9) Kobayashi, K.; Sano, Y.; Nagase, S. *J. Comput. Chem.* **2001**, *22*, 1353–1358.
(10) (a) Campanera, J. M.; Bo, C.; Olmstead, M. M.; Balch, A. L.; Poblet, J. M. *J. Phys. Chem. A* **2002**, *106*, 12356–12364. (b) Campanera, J. M.; Bo, C.; Poblet, J. M. *J. Org. Chem.* **2006**, *71*, 46–54. (c) Osuna, S.; Swart, M.; Campanera, J. M.; Poblet, J. M.; Sola, M. J. *Am. Soc. Chem.* **2008**, *130*, 6206–6214.
(11) Iezzi, E. B.; Duchamp, J. C.; Harich, K.; Glass, T. E.; Lee, H. M.; Olmstead, M. M.; Balch, A. L.; Dorn, H. C. *J. Am. Chem. Soc.* **2002**, *124*, 524–525.
(12) Lee, H. M.; Olmstead, M. M.; Iezzi, E.; Duchamp, J. C.; Dorn, H. C.; Balch, A. L. *J. Am. Chem. Soc.* **2002**, *124*, 3494–3495.
(13) Stevenson, S.; Stephen, R. R.; Amos, T. M.; Cadorette, V. R.; Reid, J. E.; Phillips, J. P. *J. Am. Chem. Soc.* **2005**, *127*, 12776–12777.
(14) Cardona, C. M.; Kitaygorodskiy, A.; Ortiz, A.; Herranz, M. A.; Echegoyen, L. *J. Org. Chem.* **2005**, *70*, 5092–5097.
(15) Cai, T.; Ge, Z.; Iezzi, E. B.; Glass, T. E.; Harich, K.; Gibson, H. W.; Dorn, H. C. *Chem. Commun.* **2005**, 3594–3596.
(16) Cai, T.; Slebodnick, C.; Xu, L.; Harich, K.; Glass, T. E.; Chancellor, C.; Fettinger, J. C.; Olmstead, M. M.; Balch, A. L.; Gibson, H. W.; Dorn, H. C. *J. Am. Chem. Soc.* **2006**, *128*, 6486–6492.
(17) Cai, T.; Xu, L.; Anderson, M. R.; Ge, Z.; Zuo, T.; Wang, X.; Olmstead, M. M.; Balch, A. L.; Gibson, H. W.; Dorn, H. C. *J. Am. Chem. Soc.* **2006**, *128*, 8581–8589.
(18) Wakahara, T.; Iiduka, Y.; Ikenaga, O.; Nakahodo, T.; Sakuraba, A.; Tsuchiya, T.; Maeda, Y.; Kako, M.; Akasaka, T.; Yoza, K.; Horn, E.; Mizorogi, N.; Nagase, S. *J. Am. Chem. Soc.* **2006**, *128*, 9919–9925.
(19) Chen, N.; Zhang, E. Y.; Tan, K.; Wang, C. R.; Lu, X. *Org. Lett.* **2007**, *9*, 2011–2013.
(20) Cardona, C. M.; Elliott, B.; Echegoyen, L. *J. Am. Chem. Soc.* **2006**, *128*, 6480–6485.
(21) Pinz, J. R.; Plonska-Brzezinska, M. E.; Cardona, C. M.; Athans, A. J.; Gayathri, S. S.; Guldi, D. M.; Herranz, M. A.; Martin, N.; Torres, T.; Echegoyen, L. *Angew. Chem., Int. Ed.* **2008**, *47*, 1–6.

Scheme 1. Synthesis of a Dibenzyl-Adduct of $Sc_3N@C_{80}$-I_h

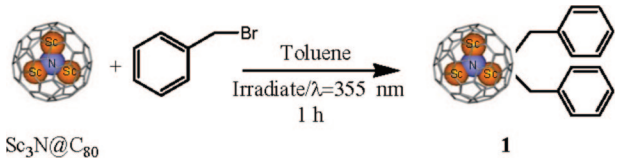

Photochemical reactions are very useful for functionalizing less-reactive species by producing highly co-reactive free radicals.[28] Herein, we report the synthesis of a dibenzyl adduct of $Sc_3N@C_{80}$-I_h in high yield and high selectivity via a photochemical reaction; this synthetic method was also applied to $Lu_3N@C_{80}$-I_h, producing a dibenzyl analogue. In contrast, when we tried the reaction with C_{60} under the same conditions, a mixture of multiadducts was obtained, indicating that this method on highly reactive species is not easily controlled. Fortunately, information on the 1,4-dibenzyl and 1,2-dibenzyl adducts of C_{60} from electrosynthesis was available from the literature[29,30] for comparison. We also find that the benzylic substituents attenuate the electronic properties of the metallofullerene in a manner similar to disilirane[18] and trifluoromethyl moieties.[27]

Results and Discussion

Synthesis and Purification of the Dibenzyl Derivative of $Sc_3N@C_{80}$-I_h. A deoxygenated solution of $Sc_3N@C_{80}$-I_h and 1000 equiv of benzyl bromide in toluene was irradiated at 355 nm without cooling for 1 h (Scheme 1). HPLC analysis indicated that a new compound was obtained in a high yield (82%) based on consumed $Sc_3N@C_{80}$-I_h (Figure 1, retention time 17.3 min). This fraction was easily isolated using a 2-(1′-pyrenyl)ethyl silica (PYE) column, and the pure final product (**1**) was obtained on a pentabromobenzyloxypropyl silica (PBB) column (Figure 2a and b) by separation from minor impurities observed at short elution times (~11 and 14 min) in Figure 1.

The positive-ion matrix assisted laser desorption ionization time-of-flight (MALDI-TOF) mass spectrum of **1** exhibits a molecular ion peak at *m*/*z* 1292 (Figure 2c), accounting for the production of the diadduct $Sc_3N@C_{80}(CH_2C_6H_5)_2$ (**1**). The peaks at *m*/*z* 1201 and 1110 are attributed to the fragments $Sc_3N@C_{80}(CH_2C_6H_5)$ and $Sc_3N@C_{80}$ formed by sequential loss of the exohedral functional groups from **1** under the laser desorption conditions as often observed with fullerenes.[16]

(22) Cardona, C. M.; Kitaygorodskiy, A.; Echegoyen, L. *J. Am. Chem. Soc.* **2005**, *127*, 10448–10453.
(23) Lukoyanova, O.; Cardona, C. M.; Rivera, J.; Lugo-Morales, L. Z.; Chancellor, C. J.; Olmstead, M. M.; Rodriguez-Fortea, A.; Poblet, J. M.; Balch, A. L.; Echegoyen, L. *J. Am. Chem. Soc.* **2007**, *129*, 10423–10430.
(24) Cai, T.; Xu, L. S.; Gibson, H. W.; Dorn, H. C.; Chancellor, C. J.; Olmstead, M. M.; Balch, A. L. *J. Am. Chem. Soc.* **2007**, *129*, 10795–10800.
(25) Iezzi, E. B.; Cromer, F.; Stevenson, P.; Dorn, H. C. *Synth. Met.* **2002**, *128*, 289–291.
(26) Shu, C. Y.; Cai, T.; Xu, L. S.; Zuo, T. M.; Reid, J.; Harich, K.; Dorn, H. C.; Gibson, H. W. *J. Am. Chem. Soc.* **2007**, *129*, 15710–15717.
(27) Shustova, N. B.; Popov, A. A.; Mackey, M. A.; Coumbe, C. E.; Phillips, J. P.; Stevenson, S.; Strauss, S. H.; Boltalina, O. V. *J. Am. Chem. Soc.* **2007**, *129*, 11676–11677.
(28) Krusic, P. J.; Wasserman, E.; Keizer, P. N.; Morton, J. R.; Preston, K. F. *Science* **1991**, *254*, 1183.
(29) Zheng, M.; Li, F. F.; Shi, Z. J.; Gao, X.; Kadish, K. M. *J. Org. Chem.* **2007**, *72*, 2538–2542.
(30) Kadish, K. M.; Gao, X.; Van Caemekbecke, E.; Suenobu, T.; Fukuzumi, S. *J. Phys. Chem. A* **2000**, *104*, 3878–3883.

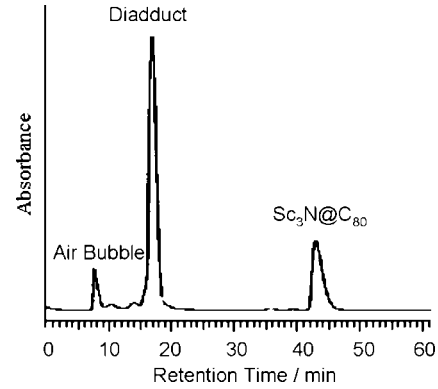

Figure 1. HPLC profile of the reaction mixture. Conditions: 10 mm × 250 mm PYE column at a flow rate of 2 mL/min with toluene as eluent.

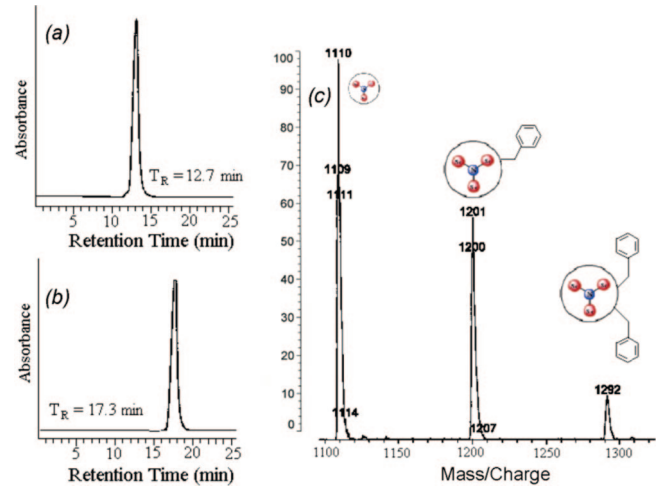

Figure 2. HPLC profiles of (a) pure product **1** on a 4.6 mm × 250 mm PBB column and (b) a 10 mm × 250 mm PYE column at flow rates of 2 mL/min with toluene as eluent. (c) Positive-ion mode MALDI-TOF mass spectrum using a 9-nitroanthracene matrix.

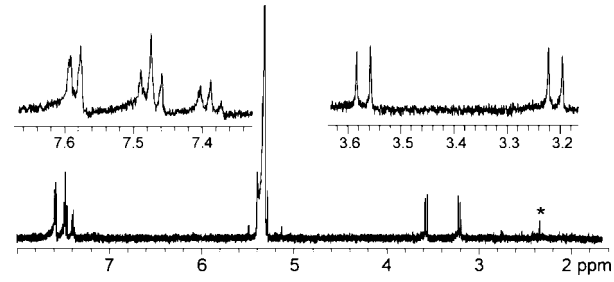

Figure 3. 500 MHz ^{1}H spectrum of **1** in CD_2Cl_2/CS_2 (v/v = 1:4). The asterisk denotes an impurity, toluene.

Determination of the Structure of the Dibenzyl Derivative of $Sc_3N@C_{80}$-I_h. The ^{1}H spectrum of diadduct **1** (Figure 3) exhibits only one set of signals for the benzyl groups: an AB quartet comprised of doublets at 3.57 ($^2J_{H-H}$ = 13 Hz) and 3.21 ppm ($^2J_{H-H}$ = 13 Hz) for the geminal hydrogens of the two equivalent methylene groups and signals for the phenyl group hydrogens at 7.38−7.59 ppm. Implementation of ^{1}H−^{1}H COSY along with heteronuclear multiple quantum coherence (HMQC) NMR on **1** verified that the two sets of nonequivalent, diastereotopic methylene hydrogens are attached to equivalent carbon atoms of a symmetric adduct (Figures S1 and S2). Therefore, the dibenzyl adduct **1** is highly symmetric.

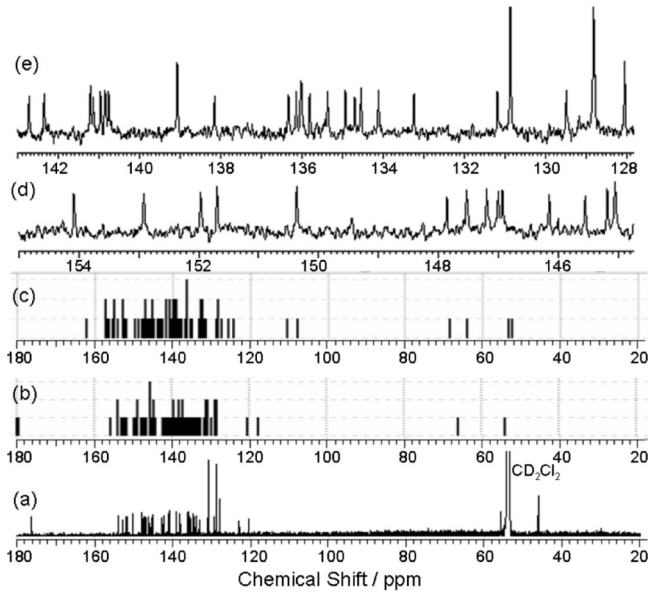

Figure 4. (a) 150 MHz ^{13}C NMR spectrum of **1** in CD_2Cl_2/CS_2 (v/v = 1:4); (b) computed (OPBE/6-311G level) ^{13}C NMR spectrum of **1d** isomer; (c) computed (OPBE/6-311G level) ^{13}C NMR spectrum of **1b** isomer; expanded regions of the experimental spectrum from (d) 155−145 ppm and (e) 143−128 ppm.

Scheme 2. Possible Regioisomeric Diadducts of $Sc_3N@C_{80}$-I_h, Reading from Left to Right: 1,2(ab)-adduct (**1a**), 1,2(aa)-adduct (**1b**), 1,4(bb)-adduct (**1c**), and 1,4(aa)-adduct (**1d**)

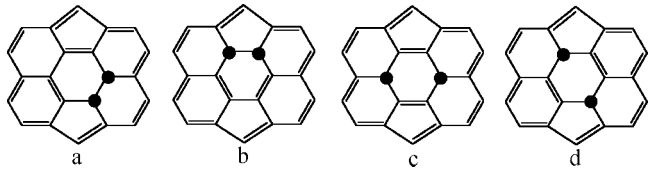

As illustrated in Scheme 2, there are four possible reaction sites on the $Sc_3N@C_{80}$-I_h cage, leading to either a 1,2-adduct on the 6,6-ring junction (**1a**), a 1,2-adduct on the 5,6-ring junction (**1b**), a 1,4-adduct on the [666] junctions (**1c**), or a 1,4-adduct on the [566] junctions (**1d**). In **1a** the two benzylic groups are nonequivalent and therefore will exhibit two distinct signals for the methylene protons. In contrast, **1c** will display a singlet for the four equivalent methylene hydrogens on the benzylic groups. In the observed ^1H spectrum of **1** (Figure 3), only one set of benzylic proton signals with nonequivalent methylene protons was observed. Thus, both structures **1a** and **1c** can be ruled out, leaving **1b** and **1d** as possibilities.

Figure 4 shows the experimental ^{13}C NMR spectrum of **1** in CS_2/CD_2Cl_2 and simulated spectra of isomers **1d** and **1b** from OPBE/6-311G level calculations.[31] From an overall comparison it can be seen that the simulated spectrum of **1d** (Figure 4b) matches the experimental spectrum (Figure 4a) reasonably well, while the computed ^{13}C NMR spectrum of isomer **1b** (Figure 4c) is dramatically different. Hence, we proceed on the basis that the observed product is **1d**. More specifically two lines are seen experimentally in the region of the sp^3 carbons (Figure 4a). One resonance at 46.30 ppm is for the methylene carbons (C85 and C88 in Figure 5b), confirmed by an HMQC spectrum, and the other at 55.96 ppm is for the two sp^3 carbons of the C_{80} cage (C83 and C84 in Figure 5b). As for the resonances of the sp^2 carbons, a total of 43 lines are observed (Figure 4a), four of which are assigned to the phenyl carbons and located at 139.07, 130.86, 128.81, and 128.04 ppm, similar to a C_{60} analogue.[30] The remaining 39 lines from 176.24 to 120.47 ppm are assigned to sp^2 carbons of the C_{80} cage. These results are in good agreement with the theoretically predicted total of 45 lines for a 1,4-adduct of $Sc_3N@C_{80}$ with C_2 symmetry. Notably, the line at 176.24 ppm is for C66 and C76 at the [566] junction, whereas the upfield line at 120.47 ppm is for C65 and C67 at the [666] junction (Figure 5b). These values agree reasonably well with the calculated shifts of isomer **1d** (Figure 4b): 179.46/180.18 and 117.74/120.65 ppm, correspondingly. In contrast, the ^{13}C NMR spectrum of $Sc_3N@C_{80}$-I_h contains resonances at 144.6 ppm for carbons at [566] junctions and 137.2 ppm for carbons at [666] junctions,[7] indicating that the functional groups do dramatically change the properties of nearby carbons. We also tried to simulate the ^{13}C NMR spectra of isomer **1d** using B3LYP/6-31G* and OLYP/6-31G(d) methods and found that the corresponding carbons' chemical shifts appeared at 173.29/174.32 and 111.73/114.46 ppm for the former and 175.99/176.60, 118.06/120.76 ppm for the latter (Supporting Information, Table 2). These results suggest that OLYP and OPBE methods based on higher basis sets may provide a better estimate of the effect of pi-stacking on NMR spectra.[31] However, in the case of the sp^3-hybridized carbons, the shifts calculated using B3LYP/6-31G* (49.78/49.59, 58.17/58.01 ppm) are much closer to the experimental data (46.30, 55.96 ppm) than those derived from OLYP/6-31G(d) (60.41/60.23, 69.54/69.41 ppm) and OPBE/6-311G (54.12/53.93, 66.20/66.08) methods (Supporting Information, Table 2). In any case, results of simulated ^{13}C NMR spectra from the three different computational methods suggest the 1,4-adduct structure **1d**, which has been unambiguously confirmed by X-ray crystallographic analysis. This high regioselectivity may be related to the Mayer bond order (MBO), pyramidalization angles of carbons[10] and the electron-donating character of the functional groups.

Figure 5 shows the geometrically optimized structures of isomers **1b** and **1d**. The calculated C83−C98 distance in the 1,2(aa)-isomer **1b**, 1.669(83) Å, is substantially elongated compared to the average C−C distance [1.437(15) Å] in unaltered 6:5-ring junctions of the starting material, $Sc_3N@C_{80}$-I_h;[7] the proximal benzylic functional groups increase the steric hindrance and make it thermodynamically unstable relative to the 1,4(aa)-isomer **1d** (see below). In contrast, the average C−C distances in the 6:5 ring junctions (C66−C83, C76−C84), 1.546(53) Å, and the 6:6 ring junctions (C67−C84, C65−C83), 1.520(57) Å, of **1d** are less elongated relative to the corresponding bonds in the starting material [1.437(15) Å for the 6:5-junction and 1.421(18) Å for the 6:6-junction], leading to deformation of the cage structure and the corresponding change of symmetry from I_h to C_2. These conclusions are confirmed by X-ray crystallographic analysis (below).

The DFT calculations revealed somewhat higher HOMOs and LUMOs for the **1d** isomer (−4.94/−2.93 eV) than the **1b** isomer (−5.00/−3.08 eV), leading to a larger HOMO−LUMO gap for **1d**. Notably, **1d** is favored thermodynamically by 10.44 kcal/mol relative to **1b**, thus supporting our assignment of structure **1d** to the product of the reaction. The introduction of a double bond in a pentagon of C_{60} increases the energy of the 1,4-adduct by about 8 kcal/mol with respect to addition of hydrogen in the

(31) (a) Taylor, R.; Hare, J. P.; Abdulsada, A. K.; Kroto, H. W. *J. Chem. Soc. Chem. Commun.* **1990**, 1423–1424. (b) Wu, A.; Zhang, P.; Xu, X.; Yan, W. *J. Comput. Chem.* **2007**, *28*, 2431–2442. (c) Magyarfalvi, G.; Pulay, P. *J. Chem. Phys.* **2003**, *119*, 1350–1357. (d) Helgaker, T.; Jaszunski, M.; Ruud, K. *Chem. Rev.* **1999**, *99*, 293–352.

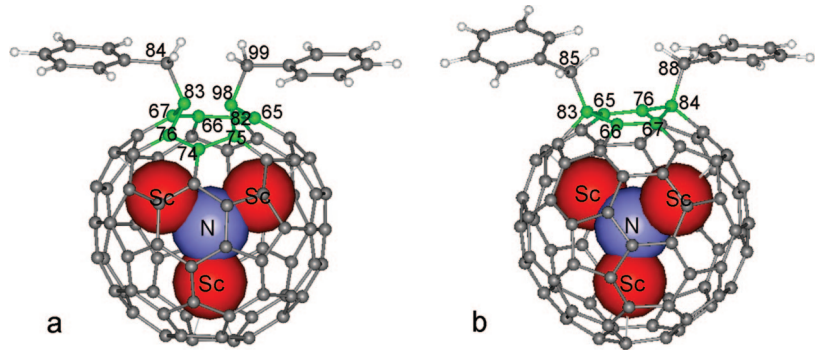

Figure 5. Geometrically optimized, thermodynamically stable structures of (a) the 1,2(aa)-adduct, **1b** and (b) the 1,4(aa)-adduct, **1d**, respectively.

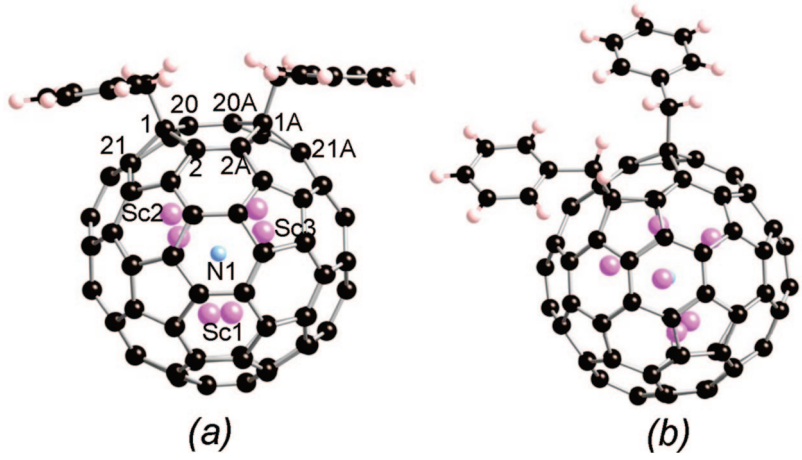

Figure 6. Two views of $Sc_3N@C_{80}(CH_2C_6H_5)_2$ (**1**) from the X-ray crystal structure showing the two positions of the disordered Sc_3N cluster. The solvate molecules are omitted for clarity.

1,2-adduct.[32,33] However, the steric hindrance from the benzylic substituents in the 1,2-adduct overrides the favorable electronic energy and makes the 1,4-adduct of C_{60} highly favored.[30]

Black needle-like single crystals of **1**·toluene suitable for X-ray crystallographic analysis were obtained by slow evaporation of a toluene solution. Although the molecules have C_2 symmetry, 2-position disorder in the packing of the C_{80} cages and the Sc_3N cluster generates crystallographic mirror symmetry. As Figure 6 shows, the benzyl groups and the eight atoms (C1, C1A, C2, C2A, C20, C20A, C21, C21A) of the C_{80} cluster that are closest to the benzyl substituents are ordered across this crystallographic mirror plane, thus unambiguously confirming the product as the 1,4(aa)-adduct of $Sc_3N@C_{80}$. The C_{80} cages and the Sc_3N cluster in the crystal are disordered. As seen in Figure 5a, the bond distances C1−C2 (1.525(11) Å) and C1−C21 (1.528(10) Å) at the 5:6-ring junction and C1−C20 (1.521 (10) Å) at the 6:6-ring junction close to the benzyl substituents are substantially elongated when compared to the average C−C distances (1.437(15) Å for 6:5-ring junctions and 1.421(18) Å for the 6:6-ring junctions)[7] of $Sc_3N@C_{80}$-I_h. The shortest Sc−C distance (Sc3−C63) is 2.0669(4) Å, shorter than that of pristine $Sc_3N@C_{80}$-I_h (2.188(9) Å, indicating that the functional group leads to distortion of the carbon cage. However, the Sc_3N cluster is still planar; the sum of the angles is 359.7(3)°.

As shown in Figure 7, the UV−vis absorption spectrum of **1d** in toluene contains a maximum at 898 nm (1.38 eV), whereas

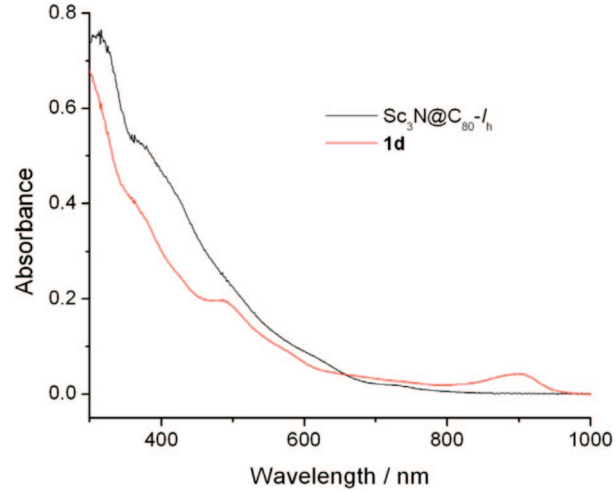

Figure 7. UV−vis spectra of **1d** (red line) and $Sc_3N@C_{80}$-I_h (gray line) in toluene.

that of $Sc_3N@C_{80}$-I_h exhibits a maximum at 735 nm (1.69 eV), in agreement with the literature.[34] This large difference in the absorption spectra is ascribed to the change of the electronic structure of the cage brought about by the removal of two p orbitals from the π system of the cage and electron donation from the benzylic substituents to the cage. These results reveal that benzylation is effective for tuning the electronic character of $Sc_3N@C_{80}$.

(32) Matsuzawa, N.; Dixon, D. A.; Fukunaga, T. *J. Phys. Chem.* **1992**, *96*, 7594.
(33) Cahill, P. A.; Rohlfing, C. M. *Tetrahedron* **1996**, *52*, 5247.
(34) Krause, M.; Dunsch, L. *ChemPhysChem* **2004**, *5*, 1445–1449.

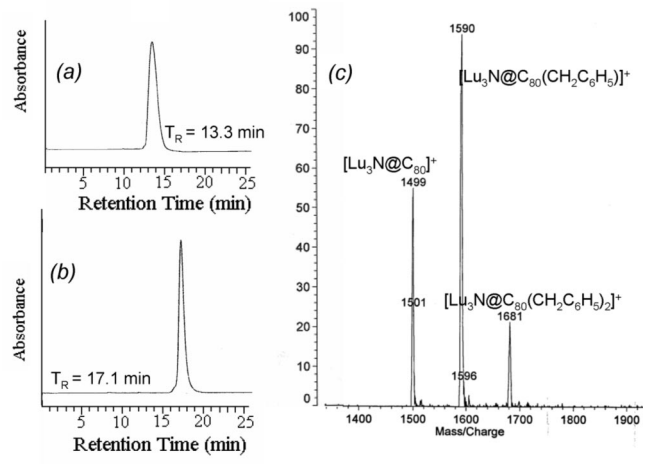

Figure 8. HPLC profiles of pure $Lu_3N@C_{80}(CH_2C_6H_5)_2$ (a) on a 4.6 mm × 250 mm PBB column and (b) on a 10 mm × 250 mm PYE column at flow rates of 2 mL/min with toluene as eluent. (c) Positive ion mode MALDI-TOF mass spectrum using a 9-nitroanthracene matrix.

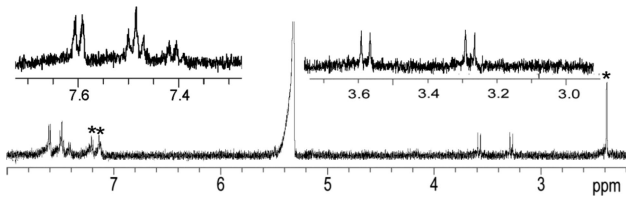

Figure 9. 500 MHz ^{1}H spectrum of $Lu_3N@C_{80}(CH_2C_6H_5)_2$ in CD_2Cl_2/CS_2 (v/v = 1:4). The asterisk denotes an impurity, toluene.

Synthesis and Characterization of the Dibenzyl Derivative of $Lu_3N@C_{80}$-I_h. $Lu_3N@C_{80}$ is a potential X-ray contrast agent;[35] therefore, functionalization of the cage surface to imbue good solubility is of great importance. Following the same reaction and purification protocols as for **1**, $Lu_3N@C_{80}(CH_2C_6H_5)_2$ was prepared in 63% yield based on unrecovered starting material. The chromatographic retention times on PBB and PYE columns are similar to those of $Sc_3N@C_{80}(CH_2C_6H_5)_2$ (Figure 8a and b), revealing that they possess similar structures. The MALDI-TOF mass spectrum of the Lu-product is shown in Figure 8c. The signal at *m*/*z* 1681 confirms that the product is the dibenzyl derivative. As for the Sc analogue, the sequential loss of the benzyl moieties leads to the signals at *m*/*z* 1590 and 1499. The ^{1}H spectrum of $Lu_3N@C_{80}(CH_2C_6H_5)_2$ (Figure 9) also exhibits only one set of signals for the benzyl groups: an AB quartet comprised of doublets at 3.58 ppm ($^2J_{H-H}$ = 13 Hz) and 3.28 ppm ($^2J_{H-H}$ = 13 Hz) for the geminal hydrogens of the two methylene groups and signals for the phenyl group protons at 7.38−7.61 ppm, very similar to the spectrum of the $Sc_3N@C_{80}$-I_h analog. The UV−vis spectrum is shown in Figure 10; as with the Sc analog, there is a maximum absorption at longer wavelength (803 nm, 1.54 eV) in the dibenzyl derivative than in the starting material (691 nm, 1.79 eV).[34] These results confirm that the addition of the benzyl substituents dramatically changes the electronic structure of the C_{80} cage.

Conclusions

In summary, a single, soluble regioisomer of $Sc_3N@C_{80}$-$(CH_2C_6H_5)_2$ was formed in high yield by photochemical activation of benzyl bromide in the presence of $Sc_3N@C_{80}$-I_h. NMR spectra revealed the C_2 symmetry of this compound: only one AB pattern was observed for the diastereotopic methylene hydrogens. We concluded that the product is the 1,4(aa)-adduct, **1d**, based on DFT calculations and the experimental data; this was confirmed by X-ray crystallography. We also prepared $Lu_3N@C_{80}(CH_2C_6H_5)_2$ in analogous manner. UV−vis spectroscopic results show that the benzylic susbstituents affect the electronic structure of the C_{80} cage, indicating that this methodology can be used in concert with changes in the encapsulated metal atoms to tune the electron-accepting properties of such materials. In addition, photochemical reactions of substituted benzyl bromides will provide access to a broad variety of metallofullerene derivatives bearing functional groups and thus allow further chemical modifications to imbue good solubility and processability.

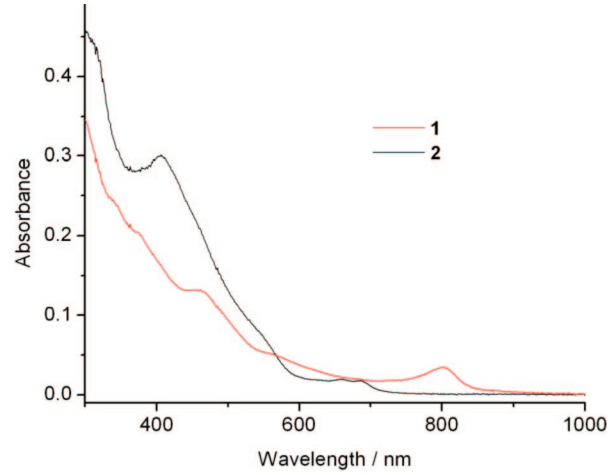

Figure 10. UV−vis spectra of $Lu_3N@C_{80}(CH_2C_6H_5)_2$, **1** (red line), and $Lu_3N@C_{80}$-I_h, **2** (black line), in toluene.

Experimental Section

Materials and Methods. A mixture of I_h and D_{5h} isomers of $Sc_3N@C_{80}$ or $Lu_3N@C_{80}$ was obtained by the chemical separation method reported in detail earlier.[36] Pure $Sc_3N@C_{80}$-I_h and $Lu_3N@C_{80}$-I_h were isolated from the mixtures by HPLC using a semipreparative PYE [β-(1-pyrenyl)ethyl silica] column (10 mm × 250 mm) with toluene at 2.0 mL/min, detector λ = 390 nm. Benzyl bromide and toluene (HPLC grade, ≥99.9%) were used as received from Aldrich. The same PYE and pentabromobenzyloxypropyl silica (PBB) columns were used for both analysis and purification of the products. HPLC system: Acure series III pump, 757 absorbance detector (Applied Biosystems). JEOL ECP 500 MHz and Bruker 600 MHz instruments were used for NMR measurements. Mass spectrometry was conducted on a Kratos Analytical Kompact SEQ MALDI-TOF mass spectrometer.

Theoretical Calculations. Geometries of **1b** and **1d** were optimized at the B3LYP level[37] using the Gaussian 03 program.[38] The effective core potential and the corresponding basis set were used for Sc. The basis sets employed were LanL2DZ[39] for Sc and 3-21G*[40] for C, H, O, and N. All the calculations were subjected to frequency analyses, which were performed at the same level as

(35) Iezzi, E. B.; Duchamp, J. C.; Fletcher, K. R.; Glass, T. E.; Dorn, H. C. *Nano Lett.* **2002**, *2*, 1187–1190.
(36) Ge, Z. X.; Duchamp, J. C.; Cai, T.; Gibson, H. W.; Dorn, H. C. *J. Am. Chem. Soc.* **2005**, *127*, 16292–16298.
(37) Becke, A. D. *Phys. Rev. A* **1988**, *38*, 3098–3100.
(38) Frisch, M. J.; et al. *GAUSSIAN 03, revision B.05*; Gaussian Inc.: Wallingford, CT, 2004.
(39) Hay, P. J.; Wadt, W. R. *J. Chem. Phys.* **1985**, *82*, 284–298.
(40) Hehre, W. J.; Ditchfield, R.; Pople, J. A. *J. Chem. Phys.* **1972**, *56*, 2257–2261.

that of the geometry optimization. As a result, no imaginary frequencies were reported for optimized structures. NMR chemical shielding tensors were evaluated employing the gauge-independent atomic orbital (GIAO) method at the B3LYP/6-31G*, OLYP/6-31G(d), and OPBE/6-311G levels of theory.[31] On the basis of the computed chemical shielding tensors, theoretical ^{13}C NMR chemical shifts were calculated relative to C_{60} and converted to the TMS (tetramethylsilane) scale using the experimental value for C_{60} (142.68 ppm).[31a]

Synthesis of $Sc_3N@C_{80}(CH_2C_6H_5)_2$ (1). A mixture of $Sc_3N@C_{80}$-I_h (10 mg, 9.0 μmol) and 1.1 mL (9.3 mmol, 10^3 equiv) of benzyl bromide in toluene (200 mL) was deoxygenated by bubbling with argon for 30 min, then irradiated in a photochemical reactor (wavelength 355 nm) without cooling for 1 h. The product was purified by HPLC with PYE and PBB columns, and the yield was estimated as 82% of **1d** from the HPLC profile.

Synthesis of $Lu_3N@C_{80}(CH_2C_6H_5)_2$. This reaction and purification were carried out analogously to the procedures outlined above for the derivative of $Sc_3N@C_{80}$.

X-ray Single Crystallography. Black needle-like crystals of **1**·toluene were obtained by slow evaporation of a toluene solution. Screening of numerous crystals suggested that the bulk sample contained polycrystalline "twins" and indexation of the reflections suggested that two orthorhombic primitive forms cocrystallized together. The approximate unit cell parameters for the two forms were (form 1) $a = 11.0$ Å, $b = 18.5$ Å, $c = 25.2$ Å, $V = 5152$ Å^3 and (form 2) $a = 11.0$ Å, $b = 15.6$ Å, $c = 29.9$ Å, $V = 5150$ Å^3. The chosen crystal, for which ~80% of reflections indexed to form 1, was centered on the goniometer of an Oxford Diffraction Nova diffractometer. The data collection routine, unit cell refinement, and data processing were carried out with the program CrysAlis.[41a] The Laue symmetry and systematic absences were consistent with the orthorhombic space groups *Pnma* and $Pn2_1a$. The structure was originally solved in both space groups using SIR92[41b] via the graphical user interface WinGX;[41c] both space groups showed disorder in the C_{80} cages and in the Sc_3N cluster, so the higher symmetry space group, *Pnma*, was chosen.

The structure was refined using SHELXTL NT.[41d] The asymmetric unit of the structure comprises 0.5 crystallographically independent $Sc_3N@C_{80}(C_7H_7)_2$ and 0.5 toluene. The molecule has crystallographically imposed mirror symmetry which can only be obtained by disorder of the C_{80} cluster. The benzyl group and the eight atoms of the C_{80} cluster that are closest to the benzyl substituent are ordered across the crystallographic mirror and were refined anisotropically. For the remainder of the atoms (i.e., 72 atoms of the C_{80} cage, the Sc_3N cluster, and the toluene), the mirror symmetry constraint was suppressed (part −1) and the relative occupancies of the disordered components set to 50:50 by symmetry. The Sc_3N cluster was refined anisotropically. A rigid group refinement was used for the disordered atoms of the C_{80} cage and the atoms were refined isotropically. The atoms of the toluene were also refined isotropically. A riding model was used for the hydrogen atoms.

Crystal Data. Crystal size 0.34 × 0.01 × 0.01 mm^3; orthorhombic; space group *Pnma*; $a = 11.0377(4)$ Å, $b = 18.4948(8)$ Å, $c = 25.2391(7)$ Å, $\alpha = 90°$, $\beta = 90°$, $\gamma = 90°$, $V = 5152.3(3)$ Å^3, $Z = 4$, $d_{calcd} = 1.784$ Mg/m^3, $F(000) = 2792$, λ (Cu Kα) = 1.54178 Å, $\mu = 3.864$ mm^{-1}, θ range for data collection 2.96−63.75°, $T = 100(2)$ K; reflections collected 19 675, independent reflections 4227 [R(int) = 0.0845], completeness to $\theta = 62.50°$, 98.7%. Refinement method: full-matrix least-squares on F^2; data/restraints/parameters: 4227/0/ 241; goodness-of-fit on F^2 1.329; final R indices [$I > 2\sigma(I)$]: R1 = 0.1281, wR2 = 0.3527; R indices (all data): R1 = 0.1738, wR2 = 0.3839; largest diff. peak and hole: 0.981 and −1.026 e·Å^{-3}.

$Sc_3N@C_{80}(CH_2C_6H_5)_2$ (1). ^1H (500 MHz, CD_2Cl_2/CS_2, 298 K): δ 3.75 (d, $J = 13$ Hz, 2H), 3.21 (d, $J = 13$ Hz, 2H), 7.38−7.59 (m, 10H); ^{13}C NMR (150 MHz, CD_2Cl_2/CS_2, doped with chromium acetylacetonate, 298 K): δ 176.24(2), 154.08(2), 152.92(2), 151.97(2), 151.69(2), 150.37(2), 147.86(2), 147.53(2), 147.19(2), 147.00(2), 146.93(2), 146.15(2), 145.55(2), 145.18(2), 145.05(2), 142.72(2), 142.35(2), 141.21(2), 141.14(2), 140.96(2), 140.85(2), 140.76(2), 139.07(2), 138.15(2), 136.32(2), 136.14(2), 136.03(2), 136.00(2), 135.81(2), 135.36(2), 134.92(2), 134.70(2), 134.54(2), 134.11(2), 133.24(2), 131.18(2), 130.86(4), 129.48(2), 128.81(4), 128.77(2), 128.04(2), 122.99(2), 120.47(2), 55.96(2), 46.30(2).

$Lu_3N@C_{80}(CH_2C_6H_5)_2$. ^1H (500 MHz, CD_2Cl_2/CS_2, 298 K): δ 3.58 (d, $J = 13$ Hz, 2H), 3.28 3.28 (d, $J = 13$ Hz, 2H), 7.42−7.61 (m, 10H).

Acknowledgment. We are grateful for support of this work by the National Science Foundation [DMR-0507083] and the National Institutes of Health [1R01-CA119371-01].

Supporting Information Available: 500 MHz COSY and HMQC NMR spectra of $Sc_3N@C_{80}(CH_2C_6H_5)_2$ in CD_2Cl_2/CS_2 (1:4). 500 MHz COSY spectrum of $Lu_3N@C_{80}(CH_2C_6H_5)_2$ in CD_2Cl_2/CS_2 (1:4); geometrically optimized thermodynamically stable structures of **1b** and **1d**, together with optimized XYZ coordinates and computed ^{13}C NMR spectra relative to TMS from B3LYP/6-31G*, OLYP/6-31G(d), and OPBE/6-311G methods; complete list of authors for ref 38; X-ray crystallographic details including a CIF file for $Sc_3N@C_{80}(CH_2C_6H_5)_2$·$C_7H_8$. This material is available free of charge via the Internet at http://pubs.acs.org.

JA804909T

(41) (a) *CrysAlis v1.171*; Oxford Diffraction: Wroclaw, Poland, 2004. (b) Altomare, A.; Cascarano, G.; Giacovazzo, C.; Guagliardi, A. *J. Appl. Crystallogr.* **1993**, *26*, 343–350. (c) Farrugia, L. J. *J. Appl. Crystallogr.* **1999**, *32*, 837–8. (d) Sheldrick, G. M. *Acta Crystallogr.* **2008**, *A64*, 112–122.